Predicting atmospheric refraction with weather modeling and machine learning

Al-Younis, Wardeh; Nevarez, Christina; Voelz, David; Sandoval, Steven; Basu, Sukanta

DOI
10.1117/12.2529533

Publication date
2019

Document Version
Final published version

Published in
Laser Communication and Propagation through the Atmosphere and Oceans VIII

Citation (APA)
Al-Younis, W., Nevarez, C., Voelz, D., Sandoval, S., & Basu, S. (2019). Predicting atmospheric refraction with weather modeling and machine learning. In J. P. Bos, A. M. J. van Eijk, & S. Hammel (Eds.), *Laser Communication and Propagation through the Atmosphere and Oceans VIII* (Vol. 11133, pp. 1-8). Article 111330E (Proceedings of SPIE - The International Society for Optical Engineering; Vol. 11133). SPIE. https://doi.org/10.1117/12.2529533

Important note
To cite this publication, please use the final published version (if applicable).
Please check the document version above.

PROCEEDINGS OF SPIE

SPIEDigitalLibrary.org/conference-proceedings-of-spie

Predicting atmospheric refraction with weather modeling and machine learning

Al-Younis, Wardeh, Nevarez, Christina, Voelz, David, Sandoval, Steven, Basu, Sukanta

Wardeh Al-Younis, Christina Nevarez, David Voelz, Steven Sandoval, Sukanta Basu, "Predicting atmospheric refraction with weather modeling and machine learning," Proc. SPIE 11133, Laser Communication and Propagation through the Atmosphere and Oceans VIII, 111330E (6 September 2019); doi: 10.1117/12.2529533

SPIE.

Event: SPIE Optical Engineering + Applications, 2019, San Diego, California, United States

Predicting Atmospheric Refraction with Weather Modeling and Machine Learning

Wardeh Al-Younis,[a] Christina Nevarez,[a] David Voelz,[a] Steven Sandoval,[a] Sukanta Basu[b]
[a]New Mexico State Univ. (United States); [b]Technische Univ. Delft (Netherlands)

ABSTRACT

This work details the analysis of time-lapse images with a point-tracking image processing approach along with the use of an extensive numerical weather model to investigate image displacement due to refraction. The model is applied to create refractive profile estimates along the optical path for the days of interest. Ray trace analysis through the model profiles is performed and comparisons are made with the measured displacement results. Additionally, a supervised machine learning algorithm is used to build a predictive model to estimate the apparent displacement of an object, based on a set of measured metrological values taken in the vicinity of the camera. The predicted results again are compared with the field-imagery ones.

Keywords: Atmospheric refraction; Time-lapse imaging; Remote mobile station; Machine learning algorithms; Weather modeling.

1. INTRODUCTION

The Earth's atmosphere includes several features that affect the propagation of light. While scattering and absorption by clouds, fogs, and aerosols primarily affect the received intensity of the radiation, the clear atmosphere can affect the propagation trajectory. Refractive index gradients that occur in the atmosphere can steer or bend light rays and are responsible for the two processes known as refraction and turbulence. The index gradients are associated with changes in air density, which for optical wavelength is primarily a function of temperature gradients in the air. Turbulence causes image shimmering and blurring and is stochastic in nature with fluctuations over short time scales. On the other hand, atmospheric refraction tends to cause more deterministic, larger scale effects (e.g., image displacement) and the effects can persist from minutes to days.[1-4] Our interest here is refraction effects in the lower atmosphere which can cause distortion of objects when viewed in imaging systems or beam steering in laser systems.

At New Mexico State University, we have developed a low-cost, mobile camera system to study atmospheric refraction. One system was recently deployed at White Sands Missile Range (WSMR), New Mexico (NM) and a second system was set up at the Jornada Experimental Range (JER), NM. Both systems collect time-lapse images of distant natural targets, such as mountain ridges. A time-lapse system was previously used in Las Cruces, NM with a building as a target to study apparent diurnal image displacement due to refraction.[5] A similar system in Dayton, OH was used by Basu et al. to investigate temporal variations of the refractive index gradient.[4] Time-lapse imagery has also been used to investigate the apparent stretch and compression of objects due to atmospheric refraction lensing effects[6] and the approach has also been applied to the estimation of turbulence strength.[7]

The prediction of atmospheric refraction effects can be advantageous for many terrestrial optical applications where prior knowledge of the light's trajectory can improve the speed and accuracy of pointing and tracking functions. The goal of this paper is to investigate a numerical weather modeling method and a machine learning (ML) method for predicting image displacement due to atmospheric refraction. Numerical weather prediction is an attractive approach for our application as it is a physics-based approach and it leverages tremendous research and resources. However, it is computationally extensive and the results are subject to initial conditions and terrain characteristics. A less intensive, more empirical tactic is to apply a ML algorithm to build a predictive model based on local meteorological data. In this paper, we describe our application of numerical weather modeling and ML methods to image displacement due to refraction and compare the results with our time-lapse camera measurements.

Laser Communication and Propagation through the Atmosphere and Oceans VIII, edited by Jeremy P. Bos, Alexander M. J. van Eijk and Stephen Hammel, Proc. of SPIE Vol. 11133, 111330E
 · doi: 10.1117/12.2529533

2. METHODS

2.1 Time-lapse Image Collection and Processing

We have recently conducted sets of experiments with a time-lapse camera located at White Sands Missile Range (WSMR) in New Mexico that is pointed generally north at a natural desert landscape and a mountain range (Oscura Mountains) on the horizon. Images were collected from January 2018 to February 2018. Another camera was set up at the Jornada Experimental Range (JER) near Las Cruces, NM and was pointed west to image a mountain range (Dona Ana Mountains) and a desert valley. This system began collecting images in May 2018 and is still operating. The mountain ridgelines observed were at a distance of about 20km for JER and over 100km for WSMR.

The battery powered camera systems are easily transported and consist of a weatherproof case on a tripod that contains a Nikon D5200 camera operated in a time-lapse mode. A zoom lens is set at its maximum focal length of 400mm for the WSMR measurements and at 300mm for the JER observations. The camera is typically programmed to collect images in 5-minute intervals with a fixed 5.6 aperture F/# and automatic shutter speed. Figure 1 shows example frames of the mountain targets and valleys for the WSMR and JER experiments.

(a) (b)

Figure 1. Example frames showing the target mountains: (a) WSMR experiment and (b) JER experiment.

Weather data is also collected for the two experiments. For the WSMR experiment, online metrological data from a weather station near the target mountain were downloaded. A Davis weather station next to the camera was utilized for the JER experiment. Weather has a significant effect on the vertical temperature gradients that are primarily responsible for the atmospheric refraction effects. The weather data of interest includes the temperature, humidity, pressure, and solar radiation. These measurements are interpolated in time to align with the time-lapse image frames.

A point-tracking algorithm is implemented to measure the apparent motion of the mountain ridges in the images.[8] An area containing the far-field target in each frame is cropped, then the algorithm detects the N "best" features in the target, stores them in a feature list in descending order of "goodness" (determined by a threshold setting), and tracks them in consecutive frames. A near-field reference close to the camera is also selected and point-tracking of this feature is applied in the analysis to remove shifts in the far-field images that are due to camera platform motion. Figure 2(a) shows some selected points associated with the far-field target for the JER experiment and Fig. 2(b) shows the positions of these points in the next consecutive frame. It is apparent that the point-tracking algorithm is essentially selecting the same points in each frame. The positions of the multiple points are averaged to give a measurement of the ridge position.

After point-tracking, the near-field average pixel coordinates are subtracted from the far-field coordinates frame-by-frame to obtain the apparent position of the far-field target. Displacement of the target from frame to frame is attributed to changes in atmospheric refraction. The most significant shifts occur in the vertical direction.

(a) (b)

Figure 2. Selected tracking points for JER far-field target: (a) initial frame and (b) the following frame.

2.2 Numerical Weather Modeling and Ray Tracing

Numerical weather prediction (NWP) is a discipline where governing equations and parameterizations that describe fluid flow and other physical processes are applied to current (or previous) weather conditions to provide a future forecast. For our purposes, the model results can be used to predict the structure of the refractive index in the atmosphere. Although, an extension of the established models is required to provide higher spatial resolution along our paths of interest.[9-10] In this section, we describe our approach for using refractive index gradient data generated by numerical weather modeling and the application of ray tracing to determine corresponding image shifts. The results of the approach are compared with time-lapse measurements in section 3. The numerical weather model (called the Weather Research and Forecasting – WRF model) uses initial and boundary conditions from global-scale reanalysis datasets and topographic effects to generate the refractive gradient data for a particular location at particular time corresponding.[10] Figure 3 illustrates the refractive index gradient model results for the WSMR experiment time-lapse imaging path in the morning on February 6, 2018. The camera site is on left and the mountain ridge is on the right.

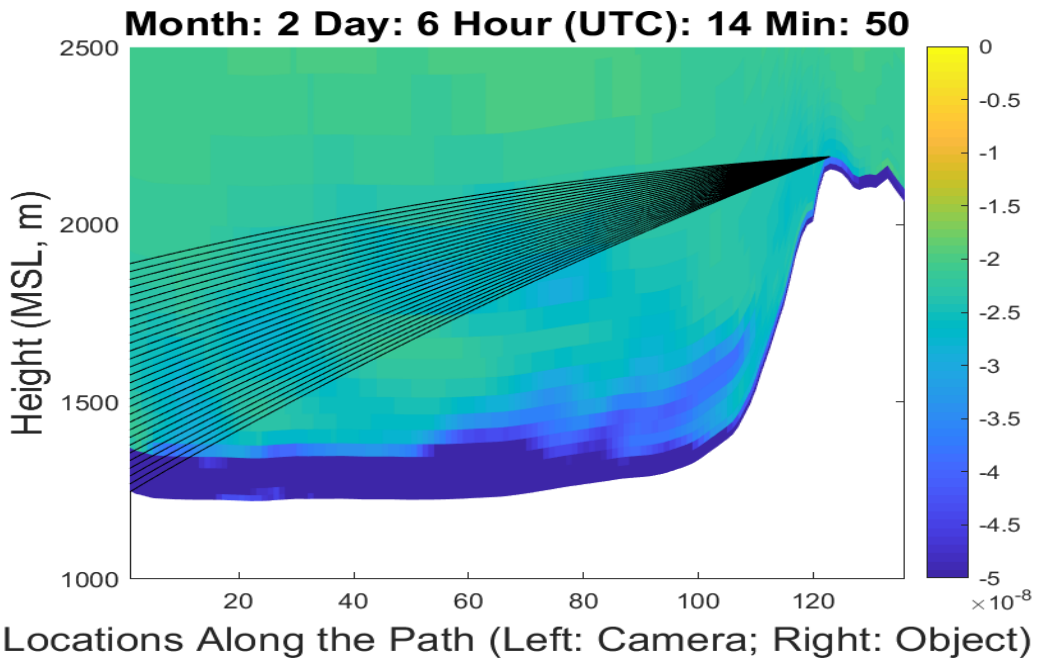

Figure 3. Example refractive index gradient results from numerical weather modeling for the WSMR experiment on February 6, 2018 at 14:50 UTC. The white area is the ground; the time-lapse camera is located in the basin on left side and a peak in the Oscura Mountains is on the right. Example ray tracing paths are shown between a position on the peak and the area near the camera.

We use ray tracing through the gradient profiles to determine the image displacements predicted by the model. Ray tracing techniques are often applied for refraction analysis over near-ground horizontal paths assuming diffraction effects are not significant. For this analysis, we apply a second-order ray tracer in a similar format as a linear ray trace analysis of optical systems, but a quadratic term is added to the transfer equation to correct the discrepancy introduced due to the linear approximation when light propagates in a graded index medium. The transfer equation describes the ray height (z) while the bending equation describes the ray angle (θ) and these are written as:

$$z(x) = \frac{x^2 \kappa}{2} + \theta_0 x + z_0 \tag{1}$$

and

$$\theta(x) = x\kappa + \theta_0 . \tag{2}$$

where θ_0 and z_0 are the initial ray angle and height, respectively. x is the propagation distance and κ is the gradient of the refractive index. Equations (1) and (2) are used in succession, to bend the ray and then provide the transfer height between planes that are within the propagation volume. Iteratively, they become,

$$z_j = \frac{\Delta x^2 \kappa(z)}{2} + \theta_{j-1} x + z_{j-1} \tag{3}$$

and

$$\theta_j = \Delta x \kappa(z) + \theta_{j-1} . \tag{4}$$

where Δx is the distance between adjacent planes and $\kappa(z)$ is the gradient value that exists between the planes. This approach assumes that the gradient value is constant between each plane.

Our ray tracing analysis approach is illustrated in Fig. 3. Rays are launched from the image target (mountain ridge on right side, elevation ~2200 m) for a range of initial angles and the ray trajectories are traced through the model gradients until they reach the ground in the basin (elevation ~ 1300 m). The specific ray that strikes the ground at the camera location is identified and we back-project a line at the ray arrival angle. The height of this line at the mountain plane indicates the apparent peak position as seen by the camera. The apparent positions are calculated for successive model frames and the relative shifts are determined.

2.3 Machine Learning Predictions

In this section, we present a ML approach to predict image displacement due to atmospheric refraction based on a set of measured metrological values. The input variables we used for prediction are temperature (T), humidity (H), pressure (P), and solar radiation (S). The predicted output is the image displacement ($\hat{y}$) due to refraction. Our weather station provides measurements of these variables at 15-minute intervals. Additionally, we utilize other local measurements available on-line at 1-hour intervals. The measurement values are normalized prior to input to the algorithm.

We considered a ML approach based on curve fitting and assumed a linear model of the form,

$$\begin{aligned} \hat{y}(T,H,P,S;\boldsymbol{w}) = {} & w_1 + w_2 T + w_3 T^2 + w_4 H + w_5 H^2 + w_6 P + w_7 P^2 + w_8 S + w_9 S^2 \\ & + w_{10} TH + w_{11} TP + w_{12} TS + w_{13} HP + w_{14} HS + w_{15} PS \end{aligned} \tag{5}$$

where $\boldsymbol{w} = [w_1 \cdots\cdots\cdots w_{15}]^T$ are the coefficient weights. Linear, square, and pairwise products of the meteorological parameters are used as non-linear kernel functions. This choice of these non-linear Kernel functions was based on experimentation.

The coefficient values $\boldsymbol{w}$ are determined by fitting Eq. (5) to training data. This can be done by minimizing an error function or cost function that measures the misfit between y for any $\boldsymbol{w}$ and the training data. Our choice of error function is the regularized squared error,

$$E(\boldsymbol{w}) = \frac{1}{2}\sum_{n=1}^{N}[\hat{y}(T_n, H_n, P_n, S_n; \boldsymbol{w}) - y_n]^2 + \frac{\lambda}{2}\|\boldsymbol{w}\|^2 \tag{6}$$

where $\boldsymbol{y} = [y_1 \cdots\cdots\cdots y_N]^T$ are the measured target values; i.e training data, and the term $(\lambda/2)\|\boldsymbol{w}\|^2$ is a penalty (regularization) term to avoid over-fitting. The value λ governs the relative importance of the regularization term compared with the squared error term.

Given N data points, $(T_n, H_n, P_n, S_n; y_n)$, the coefficients $\boldsymbol{w}$ that minimize the cost function in Eq. (6) are obtained in closed form by differentiating $E(\boldsymbol{w})$ with respect to $\boldsymbol{w}$, setting the result to zero, and solving for $\boldsymbol{w}$:

$$\boldsymbol{w} = (\lambda \boldsymbol{I} + \boldsymbol{\Phi}^H \boldsymbol{\Phi})^{-1} \boldsymbol{\Phi}^H \boldsymbol{y} \tag{7}$$

where $\boldsymbol{I}$ is the identity matrix and

$$\boldsymbol{\Phi} = \begin{pmatrix} 1 & T_1 & T_1^2 & H_1 & H_1^2 & P_1 & P_1^2 & S_1 & S_1^2 & T_1H_1 & T_1P_1 & T_1S_1 & H_1P_1 & H_1S_1 & P_1S_1 \\ 1 & T_2 & T_2^2 & H_2 & H_2^2 & P_2 & P_2^2 & S_2 & S_2^2 & T_2H_2 & T_2P_2 & T_2S_2 & H_2P_2 & H_2S_2 & P_2S_2 \\ \vdots & \vdots & \vdots & \vdots & \vdots & \vdots & \vdots & \vdots & \vdots & \vdots & \vdots & \vdots & \vdots & \vdots & \vdots \\ 1 & T_n & T_n^2 & H_n & H_n^2 & P_n & P_n^2 & S_n & S_n^2 & T_nH_n & T_nP_n & T_nS_n & H_nP_n & H_nS_n & P_nS_n \\ \vdots & \vdots & \vdots & \vdots & \vdots & \vdots & \vdots & \vdots & \vdots & \vdots & \vdots & \vdots & \vdots & \vdots & \vdots \\ 1 & T_N & T_N^2 & H_N & H_N^2 & P_N & P_N^2 & S_N & S_N^2 & T_NH_N & T_NP_N & T_NS_N & H_NP_N & H_NS_N & P_NS_N \end{pmatrix} \tag{8}$$

As illustrated in Eq. (8), the input variables are arranged as column vectors. The algorithm steps are: (1) build the matrix $\boldsymbol{\Phi}$, (2) build the vector $\boldsymbol{y}$, and (3) apply Eq. (7) to compute the weights $\boldsymbol{w}$.

3. RESULTS

Weather model data results were computed for 10-minute intervals and the ray tracing procedure was applied. The data is interpolated in time to align with the time-lapse image frames. Figure 4 shows comparative result for the WSMR experiment as a function of time-of-day where the red curve is the apparent shift (in radians) of the mountain ridge as derived from ray tracing through the weather model data. The black curve is the predicted shift by the ML algorithm where we trained the algorithm on about 500 data points of displacement and meteorological measurements collected over four days prior to the date shown. The blue curve is the shift measured in the actual camera frames. Measurements are only available for the daytime hours as the ridge cannot be seen at night.

The general downward drift throughout the daytime hours in Fig. 4 is an effect we commonly observe in clear weather and this corresponds to a reduction in the average refractive index gradient of the atmosphere along our line-of-sight. Clearly, the image shift results from the camera measurements, the weather model data, and the ML model agree particularly well in amplitude and phase, although there are differences in the short-time variations. By manually evaluating the time-lapse images, we verified that the measured variations in this case are real as opposed to noisy tracking results. These short-time excursions probably represent local fluctuations in the refractive index that are not completely captured by the weather model and it is not possible to predict these short variations by the ML model due to the differences

in sampling frequencies where the time intervals for the metrological data (1 hour) are much longer than the time-lapse intervals (5 min).

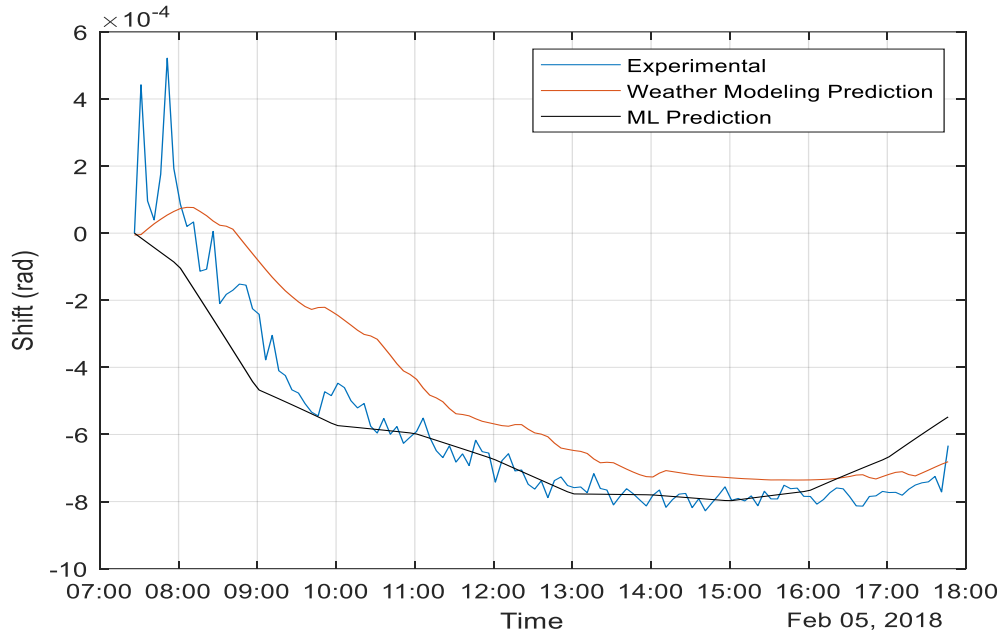

Figure 4. Data from February 2018 displaying apparent shift of the mountain peak as determined for time-lapse image data (blue), the shift as determined by ray tracing through the weather model data (red) and the shift predicted by the ML model (black).

Figure 5 presents an example ML model result for the JER experiment on a clear-day. The ML predicted result again follows a time-averaged version of the measurement. Note that the overall shift for the JER result is significantly smaller that the results for WSMR (Fig. 4). This is because the WSMR ridgeline is much further from the camera (>100 km) than for JER (20 km). Numerical weather simulation results were not currently available for the JER experiment as the mountain range is too small in width to be resolved adequately by the mesoscale model with the same resolution (~1 km) used in the WSMR experiment. For future work, we are investigating the weather simulation with at least 200 m resolution. Figure 6 presents example results for a cloudy-day for the JER experiment. Here we see the apparent shift is much smaller than for Fig. 4. However, the prediction result in Fig. 6 again is consistent with the general trend of the measurement

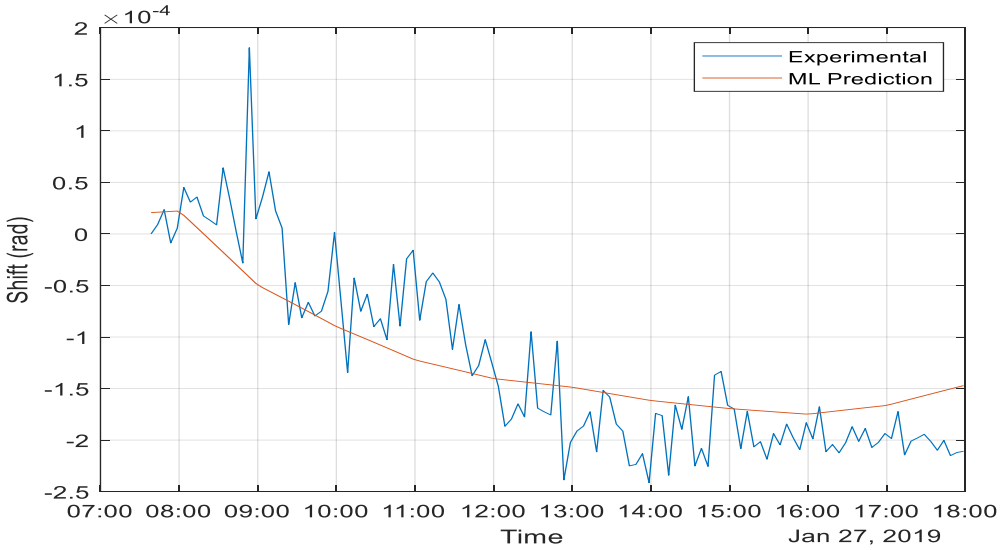

Figure 5. Clear day at JER: measured and predicted mountain ridge apparent displacement.

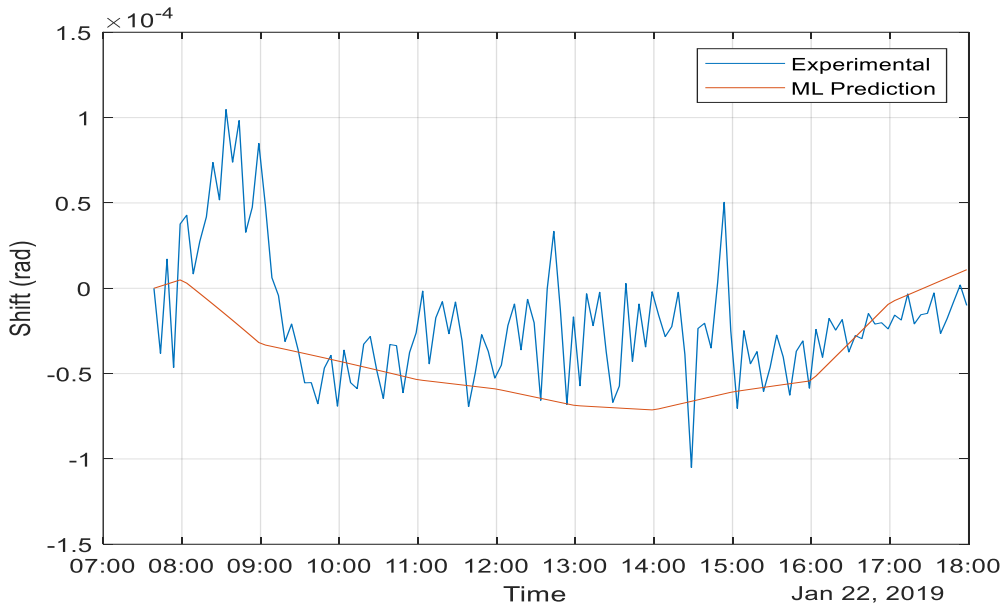

Figure 6. Cloudy day JER: measured and predicted mountain ridge apparent displacement.

4. CONCLUSIONS

We found that numerical weather simulation along with a ray tracing technique can be used for refractive effects prediction. The ray tracing approach that we applied to determine the effect of the gradients produced by the model was straightforward to implement and provided credible results. The model results of target displacement were consistent with field imagery in amplitude and phase. However, the model could not predict some of the short-time variations in field measurements, which may be due to localized events that are not completely captured by the numerical model grid or simulation process. As an alternative to numerical weather modeling, we explored the use of a ML algorithm to build a predictive model based on meteorological collected near the camera location. We found that our ML model was successful in making predictions over different weather conditions within the same meteorological season. Similar to the weather model result, the ML model prediction also could not follow the short time excursions of the field results. In this case the slow sample rate of the meteorological data compared to the time-lapse image frame rate is an aggravating factor. We are now working to determine if the model can be improved, extended and generalized so it can be applied across different seasons. We also are investigating our ability to apply image point-tracking and machine learning prediction for natural features in scenes other than ridgelines.

ACKNOWLEDGEMENTS

This work is supported by the Directed Energy Joint Transition Office (DE JTO) through grant N00014-17-12535. We thank Daniel Short, and Ivan Dragulin for collecting the White Sands time-lapse data. We also acknowledge the NMSU TAR Capstone group who constructed and operated the Jornada time-lapse system.

REFERENCES

[1] Young, A. T., “Air mass and refraction,” Appl. Opt. 33(6), 1108-1110, (1994).
[2] Auer, L. H. and Standish, E. M., “Astronomical refraction: computation for all zenith angles,” Astron. J. 119 (5), 2472-2474, (2002).

[3] Valtr, P. and Pechac, P., “Tropospheric refraction modeling using ray-tracing and parabolic equation,” Radioengineering 14(4), 98-104 (2005).
[4] Basu, S., McCrae, J. E., Fiorino, S. T., and Przelomski, J., “Estimation of temporal variations in path-averaged atmospheric refractive index gradient from time-lapse imagery,” Opt. Eng. 55(9), 090503 (2016).
[5] Voelz, D., Xiao, X., Dragulin, I., Barraza, J., Basu, S., McCrae, J. E, Pollock, Z., and Fiorino, S. T., “Low cost digital photography approach to monitoring optical bending and guiding in the atmosphere,” IEEE Aerosp. Conf. Proc, 1 –7 (2015).
[6] Short, D., Voelz, D., Barraza, J., and Dragulin, I., “Atmospheric refraction: applied image analysis and experimental example for index profile with curvature,” in Proc. SPIE 9833, Atmospheric Propagation XIII, 98330D (2016).
[7] McCrae, J. E., Bose-Pillai, S. R., and Fiorino, S. T., “Estimation of turbulence from time-lapse imagery,” Opt. Eng., vol. 56, no. 7, 071504 (2017).
[8] Al-Younis, W., Nevarez, C., and Voelz, D., “Time-lapse Imaging for Studying Atmospheric Refraction: Measurements with Natural Targets,” IEEE Aerosp. Conf. Proc, 1-7, (2019).
[9] Basu, S., Mccrae, J., Pollock, Z., He, P., Nunalee, C., Basu, S., David, D., and Fiorino, S., “Comparison of atmospheric refractive index gradient variations derived from time-lapse imagery and mesoscale modeling,” in Imaging and Applied Optics, OSA Technical Digest (online), paper PM1C.4, (2015).
[10] Basu, S., Bose-Pillai, S. R., Fiorino, S. T., and McCrae, J. E., "Evaluating a Coupled Mesoscale Modeling and Ray Tracing Framework over an Urban Area," in Imaging and Applied Optics, OSA Technical Digest, paper PW3H.3, (2018)